Interband Transitions in Sol−Gel-Derived ZrO_2 Films under Different Calcination Conditions

Sue-min Chang*,† and Ruey-an Doong‡

Institute of Environmental Engineering, National Chiao Tung University, 75, Po Ai Street, Hsinchu, 30068, Taiwan, and Department of Biomedical Engineering and Environmental Sciences, National Tsing Hua University, 101, Sec 2, Kuang Fu Road, Hsinchu, 30013, Taiwan

Received March 4, 2007. Revised Manuscript Received May 27, 2007

Different types of interband transitions as well as the microstructures and O/Zr ratios in sol−gel-derived ZrO_2 films calcined at elevated temperatures in air or N_2 were systematically examined to clarify the formation of different band structures in the structural ZrO_2 films. Optical absorptions indicate that the structural ZrO_2 films all contain direct-band transitions, while the occurrence of indirect-band and band-tail transitions depends on O/Zr ratios. Band tails mainly result from imperfect structures in the grain boundaries and appear in the ZrO_2 films with O/Zr $\geq$ 2. When the ZrO_2 films are non-stoichiometric (O/Zr $<$ 2), indirect-band transitions occur due to the folded bands caused by lattice oxygen vacancies. Monoclinic ZrO_2 has two direct-band transitions with bandgaps of 5.02−5.08 and 5.83−6.01 eV. The valence-band XPS spectra indicate that an additional occupied sub-band is located above its valence band. Indirect bandgaps in the monoclinic ZrO_2 films are in the range of 5.00−5.10 eV. Amorphous ZrO_2 films exhibit indirect-band transitions with bandgaps of 5.01−5.47 eV followed by direct-band transitions with bandgaps of 5.90−6.12 eV. In addition, tetragonal ZrO_2 contains direct bandgaps of 5.32−5.74 eV and indirect bandgaps of 4.72−5.40 eV. Size-dependent bandgaps are observed in the sol−gel-derived ZrO_2 films calcined in air, while the exponential dependence of bandgaps on O/Zr ratios is obtained in the ZrO_2 films calcined in N_2. The discrepancy is primarily due to different fates of oxygen vacancies resulting from different calcination atmospheres.

Introduction

Zirconium dioxide (ZrO_2) is a technologically important material that can be used not only in structural ceramics but also as a solid electrolyte,[1] catalyst,[2] and dielectric[3] because of its special physicochemical properties such as high ionic conductivity, surface acidity, and dielectric constant. The electronic structures of ZrO_2 including band structures and bandgaps have been reported to thermodynamically control the excitation photon energies and redox potentials in ZrO_2-based photocatalytic systems,[4,5] the energy barriers for ionic diffusion in oxygen sensors and fuel cells,[6] and the tunneling effects and functions of dielectrics in microelectronic devices.[7] Therefore, a thorough understanding of the electronic structures of ZrO_2 to better utilize such a material is thus necessarily required.

Band structures of ZrO_2 are highly dependent on chemical microstructures, particularly the crystal phases, crystallite sizes, and nature of defects.[8−10] ZrO_2 contains three kinds of polymorphs: monoclinic, tetragonal, and cubic.[11] Theoretically, the valence band of ZrO_2 is formed mainly by O 2p states with some admixing of Zr 4d states, and the conduction band is constructed primarily of Zr 4d states admixed with some O 2p states.[12] The Zr 4d states in the conduction band split into two sub-bands upon the increasing symmetry of the crystal structure from the monoclinic to the tetragonal and to the cubic form.[8] ZrO_2 is considered as a direct-bandgap material. The calculated bandgaps of the monoclinic, tetragonal, and cubic ZrO_2 are in the range of 3.12−5.42, 4.10−13.3, and 3.25−12.3 eV, respectively.[13−15] The large deviation of the calculated bandgaps is attributed to different parameters being taken into account for modeling. Quantum confinement converts the continuous-band structure to discrete electronic levels and results in the increase in the

* Corresponding author. E-mail: Chang@mail.nctu.edu.tw; tel.: +886−3-5712121 ext. 55506.
† National Chiao Tung University.
‡ National Tsing Hua University.

(1) Chen, Y. Y.; Wei, W. C. J. *Solid State Ionics* **2006**, *177*, 351.
(2) Sohn, J. R.; Lee, S. H.; Lim, J. S. *Catal. Today* **2006**, *116*, 143.
(3) Rignanese, G. M.; Gonze, X.; Jun, G.; Cho, K. J.; Pasquarello, A. *Phys. Rev. B: Condens. Matter Mater. Phys.* **2004**, *69*.
(4) Navio, J. A.; Hidalgo, M. C.; Colon, G.; Botta, S. G.; Litter, M. I. *Langmuir* **2001**, *17*, 202.
(5) Botta, S. G.; Navio, J. A.; Hidalgo, M. C.; Restrepo, G. M.; Litter, M. I. *J. Photochem. Photobiol., A* **1999**, *129*, 89.
(6) Zavodinsky, V. G. *Phys. Solid State* **2004**, *46*, 453.
(7) Miyazaki, S. *Appl. Surf. Sci.* **2002**, *190*, 66.
(8) French, R. H.; Glass, S. J.; Ohuchi, F. S.; Xu, Y. N.; Ching, W. Y. *Phys. Rev. B: Condens. Matter Mater. Phys.* **1994**, *49*, 5133.
(9) Gao, Y. F.; Masuda, Y.; Ohta, H.; Koumoto, K. *Chem. Mater.* **2004**, *16*, 2615.
(10) Emeline, A.; Kataeva, G. V.; Litke, A. S.; Rudakova, A. V.; Ryabchuk, V. K.; Serpone, N. *Langmuir* **1998**, *14*, 5011.
(11) Hannink, R. H. J.; Kelly, P. M.; Muddle, B. C. *J. Am. Ceram. Soc.* **2000**, *83*, 461.
(12) Nishizaki, T.; Okui, M.; Kurosaki, K.; Uno, M.; Yamanaka, S.; Takeda, K.; Anada, H. *J. Alloys Compd.* **2002**, *330*, 307.
(13) Orlando, R.; Pisani, C.; Roetti, C.; Stefanovich, E. *Phys. Rev. B: Condens. Matter Mater. Phys.* **1992**, *45*, 592.
(14) Zandiehnadem, F.; Murray, R. A.; Ching, W. Y. *Physica B (Amsterdam, Netherlands)* **1988**, *150*, 19.
(15) Kralik, B.; Chang, E. K.; Louie, S. G. *Phys. Rev. B: Condens. Matter Mater. Phys.* **1998**, *57*, 7027.

10.1021/cm070606n CCC: $37.00
Published on Web 08/18/2007

bandgaps upon decreasing crystallite sizes.[16] Lattice defects usually introduce extrinsic energy levels between bands and reduce bandgaps.[7] Kralik et al.[15] have predicted an occupied oxygen vacancy level positioned at 2.1 eV below the conduction-band minimum. However, most model simulations are limited to precisely describe the electronic structures of real ZrO_2 samples because complicated factors are involved.

Optical absorption is the most often adapted method to experimentally determine the band structures and bandgaps of ZrO_2. On the basis of the edges of direct band-to-band transitions, French et al.[8] have shown that the bandgaps of the monoclinic, tetragonal, and cubic phases were in the ranges of 5.83−7.09, 5.78−6.62, and 6.10−7.08 eV, respectively. Kwok and Aita[17] reported two allowed direct interband transitions with energies of 5.2 and 5.8 eV in a monoclinic ZrO_2 film. Moreover, indirect-band transitions with energies of 4.70 and 5.22 eV were found in monoclinic and tetragonal ZrO_2, respectively.[18,19] The formation of indirect-band transitions could be attributed to the existence of defects that introduce alternative energy levels between the intrinsic bands and subsequently reduce the bandgaps.[12,15] Ito et al.[20] used photoluminescence (PL) to determine the electronic structure of the ZrO_2 films deposited by plasma-enhanced vapor deposition. They reported that band-tail absorptions resulted in a PL peak around 2.8 eV. The band structures and bandgaps of ZrO_2 either obtained from experiments or obtained from model calculations are still controversial. This is attributed to the fact that different microstructures and chemical compositions of ZrO_2 usually result when they are prepared by different methods.

The sol−gel method is a promising method for nanofabrication because it is simple and feasible for structure tailoring. Moreover, ultrathin ZrO_2 films prepared using the sol−gel method have been reported.[21] Post calcination is usually required for sol−gel-derived ZrO_2 for crystallization. Calcination has been demonstrated to greatly influence the crystalline phases of ZrO_2 because of changing chemical compositions via dehydroyxlation.[22] In addition, calcination induces coalescence between crystals and results in large crystallite sizes as the temperature increases.[23] A calcination atmosphere has been reported to induce different crystalline phase transformations of sol−gel-derived ZrO_2 films.[22] However, the changes in the types of band transitions with respect to microstructures and defects of ZrO_2 calcined under different conditions have not been systematically studied yet.

In this study, we aimed to examine the interband transitions of sol−gel-derived ZrO_2 films calcined at elevated temperatures in air or N_2. Moreover, the crystalline structures and O/Zr ratios of ZrO_2 were determined to clarify the formation of the different band structures in pure ZrO_2 under different calcination conditions.

Experimental Procedures

Preparation and Characterization of Sol−Gel-Derived ZrO_2 Films. Smooth ZrO_2 films were prepared by spin-coating a fully hydrolyzed $ZrCl_4$/isopropyl alcohol (molar ratio of Zr/IPA = 1:90) solution on fused silica slides at 3000 rpm for 30 s for four cycles. The ZrO_2 films were then calcined at temperatures of 350−950 °C for 12 h in air or in N_2 for crystallization. The morphologies and thicknesses of the ZrO_2 films were characterized by scanning electron microscopy (SEM, Hitachi S-4700). The sol−gel-derived ZrO_2 films were smooth and had a thickness of ca. 35 nm. The microstructures of the thin films were examined by grazing incident X-ray diffraction (XRD, Philips X'Pert Pro) using Cu Kα radiation (λ = 1.5406 Å) with an incident angle at 1°. Data were acquired from the 25 to 35° 2θ position at a sampling width of 0.02° and a scanning speed of 4°/min. The absorption spectra of the ZrO_2 films were measured by a UV−vis spectrophotometer (Hitachi 3010) scanning from 800 to 190 nm. The valence-band structures and chemical compositions were characterized by X-ray photoelectron spectroscopy (XPS) (Physical Electronics, ESCA PHI 1600) using an Al Kα X-ray source (1486.6 eV). Argon etching operated at 3 kV was used to remove a 2 nm thickness from the top of the thin films. The photoelectrons were collected in the analyzer with a passing energy of 23.5 eV and a collection step of 0.1 eV. The shift of the photoelectron peaks in the XPS spectra resulting from charging effects was referenced to the O 1s line taken as 530.2 eV.

Dependence of Absorption Coefficients on Photon Energies. To evaluate types of absorptions, the dependence of absorbance (A) on wavelength (λ (nm)) can be converted into absorption coefficient (α (cm^{-1})) and photon energies (E (eV)) using the following equations:[24]

$$\alpha = (A \times \ln 10)/d \tag{1}$$

$$E = \frac{1240}{\lambda} \tag{2}$$

where d is the film thickness (cm) determined from the cross-sectional view of the SEM image.

Tail and Interband Absorptions. In the case of the existence of band tails, the absorption coefficients and photon energies can be fitted using the following equation that expresses Urbach tail absorption:[25]

$$\alpha = \alpha_0 \exp\left(\frac{E - E_g}{E_0}\right) \tag{3}$$

where α_0 is a constant, E_g is the bandgap, and E_0 is the inverse logarithmic slope of the absorption coefficient. Interband transitions in the functional absorption regions can be expressed using eq 4:[26]

$$\alpha E = \text{const}(E - E_g)^n \tag{4}$$

where n is the polynomial number, which is 1/2 and 2 for direct- and indirect-band transitions, respectively.

Results

Crystalline Properties and Chemical Compositions. The crystalline properties and chemical compositions of ZrO_2

(16) Liu, F. X.; Yang, J. L.; Zhao, T. P. *Phys. Rev. B: Condens. Matter Mater. Phys.* **1997**, *55*, 8847.
(17) Kwok, C. K.; Aita, C. R. *J. Appl. Phys.* **1989**, *66*, 2756.
(18) Aita, C. R.; Kwok, C. K. *J. Am. Ceram. Soc.* **1990**, *73*, 3209.
(19) Aita, C. R.; Hoppe, E. E.; Sorbello, R. S. *Appl. Phys. Lett.* **2003**, *82*, 677.
(20) Ito, T.; Maeda, M.; Nakamura, K.; Kato, H.; Ohki, Y. *J. Appl. Phys.* **2005**, *97*, 54104.
(21) Chang, S. M.; Doong, R. A. *Thin Solid Films* **2005**, *489*, 17.
(22) Chang, S. M.; Doong, R. A. *Chem. Mater.* **2005**, *17*, 4837.
(23) Stefanic, G.; Music, S. *Croat. Chem. Acta* **2002**, *75*, 727.
(24) Kosacki, I.; Petrovsky, V.; Anderson, H. U. *Appl. Phys. Lett.* **1999**, *74*, 341.
(25) Urbach, F. *Phys. Rev.* **1953**, *92*, 1324.
(26) Pankove, J. I. *Optical Processes in Semiconductors*; Dover Publications, Inc: New York, 1971.

Table 1. Crystalline Phases, Crystallite Sizes, O/Zr Ratios, and Direct and Indirect Bandgaps of Sol−Gel-Derived ZrO_2 Films Calcined in Air

T (°C)	phase	*D* (nm)[a]	O/Zr ratio	E_d (eV)	E_i (eV)
as-prepared	A[b]		2.56	5.92	
350	A		1.88	5.90	5.01
400	T[c]	15.4	1.80	5.74	5.40
450	T	15.4	1.80	5.71	5.40
500	T	16.3	1.86	5.66	5.40
700	M[d]	18.0	1.98	6.01, 5.08	
750	M	18.4	2.10	5.83, 5.02	
850	M	15.8	1.87	5.98, 5.03	5.00
950	M	15.6	1.74	5.97, 5.02	5.10

[a] Crystallite sizes of $(101)_t$ or $(111)_m$ profiles. [b] Amorphous ZrO_2. [c] Tetragonal ZrO_2. [d] Monoclinic ZrO_2.

Table 2. Crystalline Phases, Crystallite Sizes, O/Zr Ratios, and Direct and Indirect Bandgaps of Sol−Gel-Derived ZrO_2 Films Calcined in N_2

T (°C)	phase	*D* (nm)[a]	O/Zr ratio	E_d (eV)	E_i (eV)
350	A[b]		1.93	6.12	5.47
450	T[c]	18.5	1.88	5.70	5.08
550	T	17.5	1.86	5.65	5.10
600	T	15.7	1.80	5.43	4.76
650	T	15.4	1.68	5.32	4.72

[a] Crystallite sizes of $(101)_t$ profile. [b] Amorphous ZrO_2. [c] Tetragonal ZrO_2.

films calcined in air or N_2 at elevated temperatures were systematically examined by XRD and XPS. Detailed contents have been addressed in our previous paper.[22] Tables 1 and 2 summarize the crystalline phases, crystallite sizes, O/Zr ratios, and bandgaps of the ZrO_2 films obtained under various calcination conditions in air and in N_2, respectively. In air, the as-prepared ZrO_2 film was amorphous and then crystallized into a tetragonal phase at 400−500 °C. The tetragonal phase, which is a high-temperature polymorph but kinetically retained at low temperatures, began to transform into a monoclinic phase at 550 °C. The monoclinic phase became dominant above 700 °C. The crystallite sizes of the tetragonal phase fell in the range of 15.4−16.3 nm at 400−500 °C, and the crystallite sizes of the monoclinic phase were 15.6−18.4 nm at 700−950 °C. The O/Zr ratios ranged between 2.56 and 1.88 in the amorphous ZrO_2 films and changed to 1.80−1.86 in the tetragonal ZrO_2 films. The monoclinic ZrO_2 film had O/Zr ratios of 1.74−2.10. In N_2, amorphous ZrO_2 presented an O/Zr ratio of 1.93 at 350 °C. The ZrO_2 films crystallized in the tetragonal phase at 450 °C and had crystallite sizes of 15.4−18.5 nm at 450−650 °C. The O/Zr ratios in the tetragonal ZrO_2 films ranged from 1.68 to 1.88. As the temperature increased to above 750 °C, the monoclinic phase appeared and coexisted with the tetragonal phase in the ZrO_2 films. To further understand the optical properties of specific crystalline phases of ZrO_2, the films that exhibited a single-crystalline phase in XRD were selected for the UV−vis spectroscopic study.

Fundamental Absorptions. Different types of band transitions of ZrO_2 films were examined using an optical absorption method. Figure 1 shows the UV−vis absorption spectra of amorphous, tetragonal, and monoclinic ZrO_2 films calcined in air or in N_2 at elevated temperatures. The amorphous ZrO_2 films exhibited obvious absorptions below 225 nm when the calcination temperature was lower than 350 °C in air. A blue-shift of the absorption edge to 220 nm was observed as the ZrO_2 film crystallized into the tetragonal

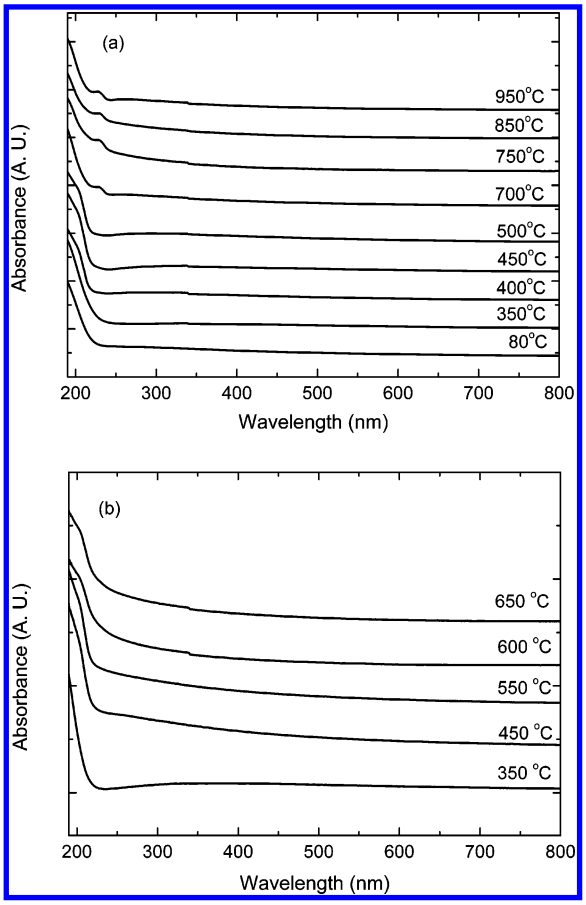

Figure 1. UV−vis absorption spectra of ZrO_2 films calcined at elevated temperatures (a) in air and (b) in N_2.

phase at 400−500 °C. The monoclinic ZrO_2 films obtained at temperatures above 700 °C exhibited shoulder absorptions with an onset of 240 nm and centered at 230 nm. The following absorptions began at 220 nm. A similar absorption behavior was observed in the amorphous and tetragonal ZrO_2 films calcined in N_2. However, the changes in the absorption edges of the structural films were different under different atmospheres. In N_2, the onset of the amorphous ZrO_2 at 350 °C was at 215 nm. After crystallization into the tetragonal phase, absorption edges continuously red-shifted to 230 nm as the temperature increased to 650 °C.

To specify the transition types of the structural ZrO_2 films, the dependence of the absorption coefficient (α (cm^{-1})) on the photon energies (E (eV)) was derived. The absorption coefficient and photon energy were converted from absorbance (A) and wavelength (λ (nm)), respectively, based on eqs 1 and 2. Because the tetragonal and monoclinic phases have been demonstrated to be stabilized at non-stochiometry (O/Zr < 2) and stochiometry (O/Zr = 2) conditions, respectively, the as-prepared ZrO_2 and films calcined at 450 and 750 °C in air were selected as typical amorphous, tetragonal, and monoclinic ZrO_2 to investigate the band structures of structural ZrO_2. Figure 2 shows the absorption coefficients as functions of photon energies of the as-prepared, tetragonal, and monoclinic ZrO_2 films and their curve fitting of the Urbach tail. As-prepared ZrO_2 displayed two functional band absorptions in the energy region of 5.00−6.53 eV with a transition at 6.20 eV. The tetragonal ZrO_2 calcined at 450 °C shifted its band absorption to the

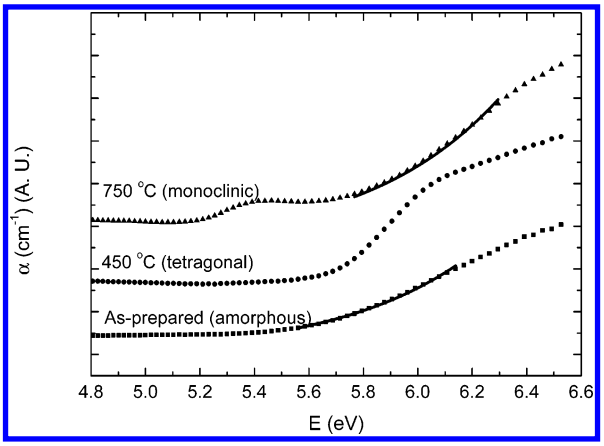

Figure 2. Optical absorption spectra of as-prepared ZrO_2 and samples calcined at 450 and 750 °C in air. Solid line represents the curve fitting of the Urbach tails.

range of 5.69−6.53 eV and was converted at 6.00 eV. In contrast, the monoclinic ZrO_2 calcined at 750 °C exhibited three functional band absorptions in the range of 5.20−6.53 eV with two transitions at 5.40 and 6.30 eV.

Figure 3 presents $(\alpha E)^2$ and $(\alpha E)^{1/2}$ as functions of E. As-prepared amorphous ZrO_2 exhibited a linear dependence of $(\alpha E)^2$ on E at 6.17−6.53 eV, which indicates the occurrence of direct band-to-band transitions. Extrapolating the linear region to the x-axis, where $(\alpha E)^2$ equals zero, yields a direct bandgap (E_d) of 5.92 eV. The tetragonal ZrO_2 film calcined at 450 °C in air presented a direct-band transition over the range of 6.00−6.53 eV and edged at 5.71 eV. After calcination at 750 °C, the monoclinic ZrO_2 film exhibited two direct transition regions, 5.20−5.37 and 6.30−6.53 eV, in which the corresponding values of $E_{d'}$ and $E_{d''}$ were 5.02 and 5.83 eV, respectively. The absorptions below the direct-band edge could be either indirect-bands or band-tail absorptions. After fitting the Urbach absorptions, we observed that the amorphous and monoclinic phases displayed an exponential dependence of α on E at values over the ranges of 5.51−6.08 and 5.78−6.30 eV, respectively (Figure 3, solid lines), which suggest the presence of Urbach tails. We could not perform such a fitting, however, to the tetragonal phase, which means that its low-energy absorption belongs to an indirect transition. Extrapolating the linear-dependence region between $(\alpha E)^{1/2}$ and E (5.74−6.00 eV) to $(\alpha E)^{1/2} = 0$ yields $E_i = 5.40$ eV.

Similar optical methods were adapted to determine the transition types and energies of the sol−gel-derived ZrO_2 films under different calcination conditions. As illustrated in Table 1, direct-band transitions were obtained in all the ZrO_2 films calcined in air. In addition, the tail absorption was only observed in the monoclinic films at 700 and 750 °C and the as-prepared amorphous ZrO_2. The tetragonal phase mainly exhibited indirect-band transitions below the direct-band absorptions. However, amorphous and monoclinic ZrO_2 at 350 and above 850 °C also presented indirect-band absorptions rather than band-tail absorptions. The amorphous ZrO_2 calcined at 350 °C in air had an indirect bandgap of 5.01 eV followed by a direct bandgap of 5.90 eV. After crystallization to tetragonal ZrO_2, the direct bandgaps decreased to 5.74−5.66 eV, while the indirect bandgaps increased to 5.40 eV. The monoclinic ZrO_2

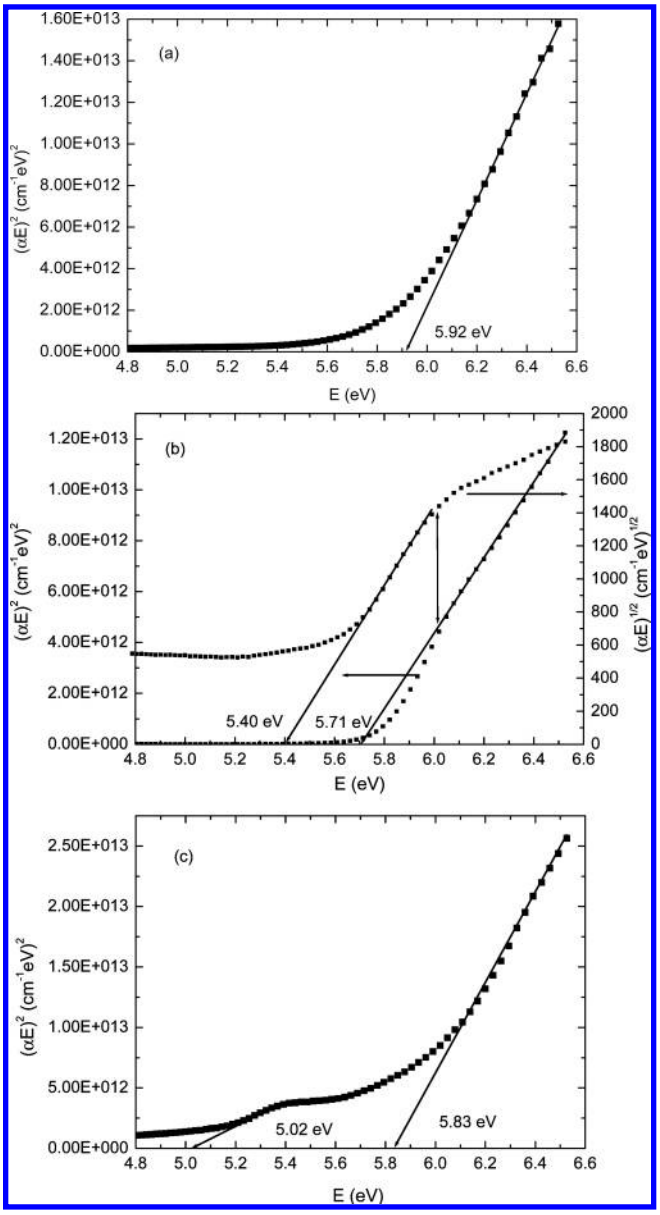

Figure 3. Plots of $(\alpha E)^2$ and $(\alpha E)^{1/2}$ of structural ZrO_2 films as functions of E. (a) As-prepared ZrO_2, (b) ZrO_2 films calcined at 450 °C (tetragonal), and (c) 750 °C (monoclinic) in air.

obtained above 700 °C presented the direct bandgaps $E_{d'}$ and $E_{d''}$ in the range of 5.02−5.08 and 5.83−6.01 eV, respectively. The indirect bandgaps of the monoclinic films calcined above 850 °C lay in the 5.00−5.10 eV range. Table 2 summarizes the bandgaps of the ZrO_2 films calcined in N_2. At 350 °C, amorphous ZrO_2 had direct and indirect bandgaps of 6.12 and 5.47 eV, respectively. At 450−650 °C, the direct and indirect bandgaps of tetragonal ZrO_2 fell in the range of 5.32−5.70 and 4.76−5.10 eV, respectively. Both the direct and the indirect bandgaps decreased upon increasing calcination temperatures.

Valence-Band XPS Spectra. To better understand the band structures of different crystalline phases of ZrO_2, we also examined the valence bands using XPS. Figure 4 presents the valence-band XPS spectra of amorphous, tetragonal, and monoclinic ZrO_2 films under different calcination conditions. The XPS spectra comprised O 2p, O 2s, and Zr 4p lines. The uppermost valence band arose mainly

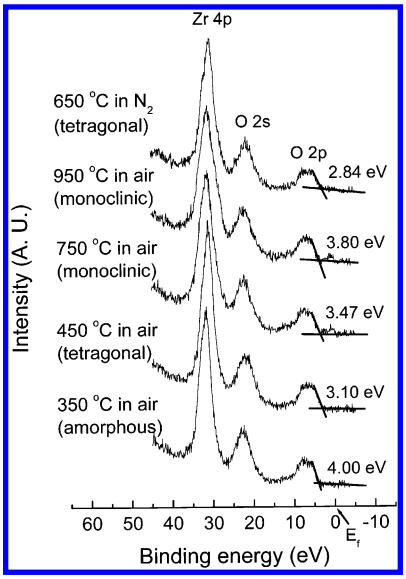

Figure 4. Valence-band XPS spectra of ZrO_2 films under different calcination conditions.

from the O 2p states, which can be divided into O 2p nonbonding states at the lower binding energy and Zr−O bonding states at the higher binding energy. O 2s and Zr 4p states constructed the lower valence bands. Except for the monoclinic ZrO_2 films obtained at 750 and 950 °C in air, similar valence-band structures were observed in the amorphous and tetragonal ZrO_2 films. These monoclinic films showed small photoelectron peaks close to the Fermi level. Morant et al.[27] found a similar peak in the ZrO_2 films after Ar ion bombardment. They considered that the peak was from the occupied oxygen vacancy state. However, we did not observe such a phenomenon in the tetragonal films, which were oxygen deficient. We thus attributed this peak to the intrinsic nature of monoclinic ZrO_2. The binding energy of the onset of the O 2p peak reveals the energy gap between the valence-band maximum and the Fermi level (E_{vf}). Amorphous ZrO_2 calcined at 350 °C in air had the highest E_{vf} value of 4.00 eV, while the E_{vf} value of monoclinic ZrO_2 was in the range of 3.47−3.80 eV. The tetragonal ZrO_2 film calcined at 450 °C in air and at 650 °C in N_2 displayed a low shift in its E_{vf} value to 2.84−3.10 eV. To determine the position of the Fermi level between bands, the energy gaps from the Fermi level to the conduction band (E_{cf}) were estimated by subtracting the E_{vf} value from the indirect bandgaps (E_i) of amorphous and tetragonal ZrO_2 and from the direct bandgap ($E_{d''}$) of the monoclinic films. The E_{cf} value of the sol−gel-derived films ranged from 1.01 to 2.30 eV. The lower E_{cf} than E_{vf} value indicates the *n*-type semiconductor nature of the sol−gel-derived ZrO_2 films. Moreover, the Fermi level is mostly close to the conduction-band minimum in amorphous ZrO_2, presumably due to the significant folding in the bands resulting from oxygen vacancies and structural randomness.

Discussion

Direct-Band, Indirect-Band, and Band-Tail Transitions. The sol−gel-derived ZrO_2 films contain direct-band and either indirect-band or band-tail transitions. The different types of band transitions occur under different calcination conditions, depending on the microstructures and O/Zr ratios. Theoretically, the valence band of ZrO_2 is mainly composed of occupied O 2p states, and the conduction band is constructed of unoccupied Zr 4d states. The Zr 4d states can be split into two sub-bands. The lower lying band is constructed of Zr 4d $x^2 - y^2$ and z^2 states, and the higher lying band is composed of Zr 4d *xy*, *yz*, and *zx* states.[8] The conduction band of ZrO_2 varies greatly upon the crystalline phases. The two sub-conduction bands merge as the crystalline phase transformed from a more symmetric cubic structure to a less symmetric monoclinic phase because of the partially octahedral crystal field.[8,28] Lucovsky et al.[29] measured the optical absorptions of a ZrO_2 film in the energy region of 5.5−9.0 eV and indicated that the energies for the first band transition, from O 2p to Zr 4d ($x^2 - y^2$, z^2), ranged from 5.5 to 6.5 eV, while the second band transition, from O 2p to Zr 4d (*xy*, *yz*, *zx*), was in the range of 6.5−8.0 eV. In this study, the direct-band absorptions from 5.32 to 5.71 eV in tetragonal ZrO_2 provide information mainly on the energy gaps of the first transitions and the band structure of the lower lying Zr 4d ($x^2 - y^2$, z^2) states.

Monoclinic ZrO_2 films were found to have two direct-band transitions with bandgaps of 4.89−5.08 and 5.78−6.01 eV in this study. Similarly, Kwok and Aita[18] also found two direct interband transitions with bandgap energies of 5.2 and 5.8 eV in monoclinic ZrO_2. However, Dash et al.[28] adapted electron energy loss spectroscopy to determine the bandgaps of monoclinic ZrO_2 and reported that below a direct bandgap of 5.3 eV was an indirect bandgap of 3.8 eV. In this study, we consider that monoclinic ZrO_2 belongs to direct-band structures because the two corresponding interband absorptions are discrete. A shoulder-like absorption reveals that an additional sub-band exists between the primary bands of monoclinic ZrO_2. Its bandwidth, determined from the peak width of the shoulder absorption, is around 0.74 eV. Moreover, a small photoelectron peak, appearing closer to the Fermi level than the O 2p states, in the valence-band XPS spectra indicates that the sub-band is constructed of occupied states and located above the primary valence band. The thin sub-band, however, is not shown in most model calculations. This discrepancy is attributed to that perfect monoclinic structures are usually used in calculations, while the formation of the sub-band could result from defects. Our previous study[22] has demonstrated that monoclinic ZrO_2 is stabilized at a stoichiometric O/Zr ratio, which means that the defect in the monoclinic phase can be the dislocation of Zr or O atoms. Foster et al.[30] have modeled the energy levels of point defects in monoclinic ZrO_2 and found that the electronic state of interstitial O^- was 0.8 eV above the top of its valence band. In this study, the energy difference between two direct bandgaps in monoclinic ZrO_2 was 0.81−

(27) Morant, C.; Sanz, J. M.; Galan, L. *Phys. Rev. B: Condens. Matter Mater. Phys.* **1992**, *45*, 1391.
(28) Dash, L. K.; Vast, N.; Baranek, P.; Cheynet, M. C.; Reining, L. *Phys. Rev. B: Condens. Matter Mater. Phys.* **2004**, *70*, 245116.
(29) Lucovsky, G.; Hong, J. G.; Fulton, C. C.; Zou, Y.; Nemanich, R. J.; Ade, H.; Scholm, D. G.; Freeouf, J. L. *Phys. Status Solidi B* **2004**, *241*, 2221.
(30) Foster, A. S.; Sulimov, V. B.; Gejo, F. L.; Shluger, A. L.; Nieminen, R. M. *J. Non-Cryst. Solids* **2002**, *303*, 101.

0.95 eV, which is close to the difference (0.8 eV) between the interstitial O^- state and the valence band. Therefore, we attribute the formation of the sub-band in monoclinic ZrO_2 to the substantial amounts of interstitial O^- defects and the shoulder adsorption to the direct-band transition from the interstitial O^- states to the Zr 4d states.

Band-tail absorptions were observed in the amorphous and monoclinic ZrO_2 films, which contain O/Zr ratios higher and almost equal to stochiometry, respectively. The occurrence of band tails in the as-prepared amorphous ZrO_2 film suggests that the tail structure is the consequence of disordered structures. Ito et al.[20] found band tails in crystalline ZrO_2 and reported that the band tails were caused by structural randomness and were irrespective of chemical compositions. Similar observations also have been reported for $FeSi_2$ films.[31] Therefore, we attribute the band tails in the monoclinic films to the imperfect structures in the grain boundary. On the other hand, the amorphous and monoclinic ZrO_2 films that have non-stoichiometric O/Zr ratios (O/Zr < 2) present indirect-band transitions rather than band-tail absoprtions. In addition, tetragonal ZrO_2 films, which are stabilized under oxygen deficient conditions, all exhibit indirect-band absorptions. This finding indicates that the indirect band primarily results from oxygen vacancies. The oxygen vacancies produced by deoxygenation at high temperatures in the monoclinic ZrO_2 films have been demonstrated to segregate from the crystalline domains to boundaries for phase stabilization.[22] Therefore, the indirect-band transitions in the monoclinic ZrO_2 films are mainly caused by the oxygen vacancies in the interstitial part between the monoclinic grains but not the intrinsic properties of the monoclinic structures. Kralik et al.[15] estimated the oxygen vacancy state in a cubic phase and reported that the occupied state is positioned 2.1 eV below the conduction-band edge. In this study, however, the indirect bandgaps ranged between 4.67 and 5.40 eV. The large indirect bandgaps imply that the indirect-band transition is not from the occupied oxygen vacancy level to the conduction band. Instead, the UV absorptions showed that the indirect-band transition is continuously followed by direct-band transitions. This result suggests that the indirect-band transitions result from the folded conduction and valence bands in different space profiles. The tetragonal model exhibited an energy difference of 0.26−0.67 eV between direct and indirect bandgaps, which is larger than the calculated value (0.17 eV)[15] obtained from the GW model for oxygen vacancy free tetragonal ZrO_2. This finding shows that substantial amounts of oxygen vacancies in the experimental tetragonal films lead to a significant folded band structure. On the basis of the results of UV absorption and XPS, the band structures of typical tetragonal and monoclinic ZrO_2 films are illustrated in Figure 5. The tetragonal ZrO_2 presents folded band structures, while the monoclinic ZrO_2 contains flat bands. As compared to tetragonal ZrO_2, monoclinic ZrO_2 has an additional thin valence band that results from interstitial O^- defects.

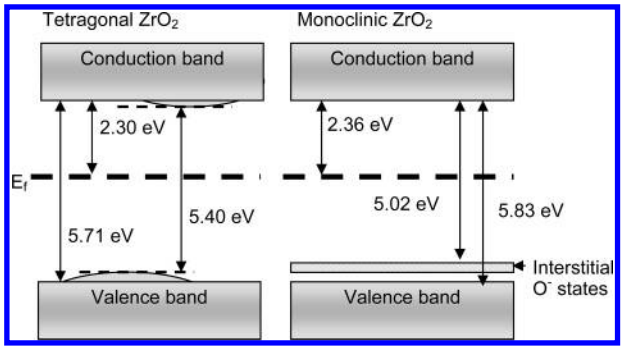

Figure 5. Typical band structures of tetragonal and monoclinic ZrO_2 films calcined at 450 and 750 °C in air, respectively.

Bandgaps. In addition to the band structures, the bandgaps of the sol−gel-derived ZrO_2 films are greatly dependent on the crystalline phases and defects. Amorphous ZrO_2 films had direct bandgaps of 5.90−6.12 eV. As they crystallized into a tetragonal form, direct bandgaps declined to 5.32−5.74 eV because of the increased crystallite sizes. The increase in direct bandgaps to 5.78−6.01 eV was observed after phase transformation from tetragonal to monoclinic forms. Similar experimental results were reported by French et al.[8] who determined the direct bandgap of 5.78−6.62 eV in the tetragonal phase and 5.83−7.09 eV in the monoclinic phase using vacuum ultraviolet (VUV) spectroscopy. However, most theoretical calculations predict a lower direct bandgap in the monoclinic phase than in the tetragonal phase. The discrepancy between experimental and modeling results is probably due to the underestimation of oxygen vacancies in the tetragonal ZrO_2.

Quantum size effects demonstrate the reduction in direct bandgaps upon increasing crystallite sizes. Kosacki et al.[24] found that a quantum effect occurred when the crystallite size was smaller than 100 nm in Y-doped ZrO_2. Moreover, the dependence of bandgaps on crystallite sizes was well-fitted by a quantum confinement model until the crystallite size was 10 nm.[24] They considered that the types of chemical bonding and stability of the crystallite lattice were responsible for the deviation of the experimental results from the model as the crystallite size was smaller than 10 nm. In this study, the size-dependent direct bandgaps were observed in most sol−gel-derived ZrO_2 films. However, exceptions occurred when lattice defects were involved in the band formation. Unlike the bandgaps between O 2p and Zr 4d states, the transition energy from the states of interstitial O^- to the conduction band in monoclinic ZrO_2 ranged from 4.89 to 5.08 eV and varied irrespectively of the crystallite sizes. It is noted that the tetragonal ZrO_2 calcined in N_2 had decreasing direct bandgaps with decreasing crystallites (see Supporting Information Figure S1). This phenomenon is opposite of the quantum size effect. We attribute the discrepancy to oxygen vacancies. In N_2, the crystallite sizes of tetragonal ZrO_2 decreased with increasing temperatures. Meanwhile, the O/Zr ratio in tetragonal ZrO_2 decreased from 1.88 to 1.68 via dehydroxylation. We found that the direct bandgaps as well as the indirect bandgaps had an exponential dependence on the O/Zr ratios (Figure 6). This finding reveals that the contents of oxygen vacancies dominate not only band structures but also bandgaps of tetragonal ZrO_2

(31) Katsumata, H.; Makita, Y.; Kobayashi, N.; Shibata, H.; Hasegawa, M.; Aksenov, I.; Kimura, S.; Obara, A.; Uekusa, S. *J. Appl. Phys.* **1996**, *80*, 5955.

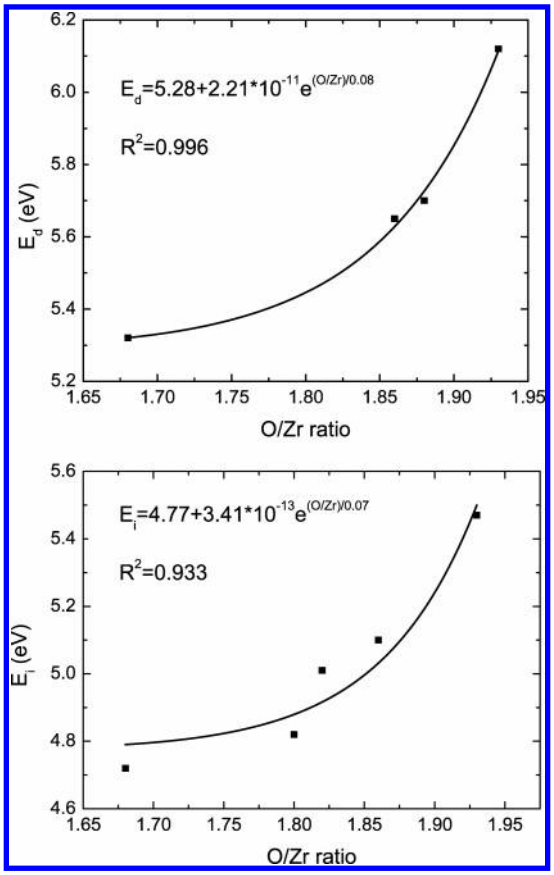

Figure 6. Dependence of (a) direct bandgaps and (b) indirect bandgaps on O/Zr ratios in tetragonal ZrO_2 films calcined in N_2.

films. Moreover, the oxygen vacancies have a significant effect on the bandgaps rather than the crystallite sizes. However, the consideration of oxygen vacancies is not taken into account in quantum confinement model calculations.

The effect that oxygen vacancies have on the band structures is insignificant in tetragonal ZrO_2 films calcined in air. The energy difference between direct and indirect bandgaps was 0.55−0.67 eV in N_2, while it was 0.26−0.34 eV in air. The larger energy difference in N_2 indicates that more remarkable folded bands resulted. Even though the ZrO_2 films contain similar crystalline characteristics and O/Zr ratios, their band structures are varied. These phenomena are attributed to different distributions of defects resulting from different fates of oxygen vacancies in different calcination atmospheres. Our previous study[22] has demonstrated that oxygen in air can be converted into oxygen ions and then diffuse into the interior of ZrO_2 films through a grain boundary to reduce the oxygen vacancies and induce the tetragonal-to-monoclinic phase transformation. In N_2, ZrO_2 lacks this external oxygen source, and the phase transformation starts from the core of the tetragonal grains via segregation of the oxygen vacancies. Therefore, it can be proposed that calcination in N_2 results in larger amounts of oxygen vacancies in the tetragonal lattice than that obtained in air. The dependence of bandgaps on O/Zr ratios and the larger difference between direct and indirect bandgaps in N_2 agree with this deduction. On the basis of the cross comparison of interband transitions, microstructures, and chemical compositions, the role of calcination conditions in dominating the electronic structures of sol−gel-derived ZrO_2 films is explicitly demonstrated in this study.

Conclusion

In this study, we clearly demonstrated that calcination conditions govern the band structures as well as bandgaps of sol−gel-derived ZrO_2 because they determine the microstructures (crystalline phases and sizes) and defects (content, types, and location). Direct-band transitions accompanied with indirect-band or band-tail transitions are observed in all sol−gel-derived ZrO_2 films. Moreover, an additional subband above the primary valence band was introduced, which is considered to be the result of interstitial O^- defects in the monoclinic ZrO_2 lattice. The occurrence of indirect-band or band-tail transitions depends on O/Zr ratios. Band tails exist in ZrO_2 films because of structural randomness when the O/Zr ratio was ≥ 2. On the other hand, indirect-band transitions occur in the ZrO_2 films with non-stochiometric O/Zr ratios (<2) because of oxygen vacancies. Lattice oxygen vacancies are responsible for indirect-band transitions in tetragonal ZrO_2 films, while boundary ones lead to such transitions in the monoclinic ZrO_2 films. Calcination atmospheres control the fate of oxygen vacancies in the ZrO_2 films, so there are different changes in bandgaps at elevated temperatures. The lack of an external oxygen source in N_2 induces a larger content of oxygen vacancies in the tetragonal lattices. Therefore, the bandgaps of tetragonal ZrO_2 are exponentially dependent on O/Zr ratios in N_2, whereas crystallite sizes dominate the energies of interband transitions in air. Results obtained in this study not only clearly demonstrate the factors governing the formation of different band structures but also provide basic information on controlling the electronic structures of ZrO_2 via calcination conditions.

Acknowledgment. The authors thank the National Science Council, Taiwan, R.O.C. for financial support under Grant NSC95-2221-E-009-110. This research was also supported by the MOE ATU Program.

Supporting Information Available: Dependence of direct bandgaps of tetragonal ZrO_2 films on crystallite size when calcined in N_2. This material is available free of charge via the Internet at http://pubs.acs.org.

CM070606N